A&A 667, L4 (2022)
https://doi.org/10.1051/0004-6361/202245018
© R. Fuentetaja et al. 2022

Astronomy & Astrophysics

LETTER TO THE EDITOR

Discovery of two new interstellar molecules with QUIJOTE: HCCCHCCC and HCCCCS⋆

R. Fuentetaja[1], M. Agúndez[1], C. Cabezas[1], B. Tercero[2,3], N. Marcelino[2,3], J. R. Pardo[1], P. de Vicente[2], and J. Cernicharo[1]

[1] Dept. de Astrofísica Molecular, Instituto de Física Fundamental (IFF-CSIC), C/ Serrano 121, 28006 Madrid, Spain
e-mail: r.fuentetaja@csic.es; jose.cernicharo@csic.es
[2] Centro de Desarrollos Tecnológicos, Observatorio de Yebes (IGN), 19141 Yebes, Guadalajara, Spain
[3] Observatorio Astronómico Nacional (OAN, IGN), C/ Alfonso XII, 3, 28014 Madrid, Spain

Received 19 September 2022 / Accepted 11 October 2022

ABSTRACT

We report on the discovery of two new molecules, HCCCHCCC and HCCCCS, towards the starless core TMC-1 in the Taurus region from the QUIJOTE line survey in the 31.1–50.2 GHz frequency range. We identify a total of twenty-nine lines of HCCCHCCC and six rotational transitions of HCCCCS. The rotational quantum numbers range from J_u = 10 up to 15 and $K_a \leq 2$ for HCCCHCCC and J_u = 21/2 up to 31/2 for HCCCCS. We derived a column density for HCCCHCCC of $N = (1.3\pm0.2)\times10^{11}$ cm^{-2} with a rotational temperature of 6±1 K, while for HCCCCS we derived $N = (9.5\pm0.8)\times10^{10}$ cm^{-2} and $T_{\rm rot} = 10\pm1$ K. The abundance of HCCCHCCC is higher than that of its recently discovered isomer, l-H_2C_6. If we compare HCCCCS with its related molecules, HCS and HCCS, we obtain abundance ratios HCS/HCCCCS = 58 and HCCS/HCCCCS = 7.2. We investigated the formation of these two molecules using chemical modelling calculations. The observed abundances can be accounted for by assuming standard gas-phase formation routes involving neutral-neutral reactions and ion-neutral reactions.

Key words. molecular data – line: identification – ISM: molecules – ISM: individual objects: TMC-1 – astrochemistry

1. Introduction

The number of molecules discovered in the cold dark cloud TMC-1, both with the Yebes 40 m radio telescope through the QUIJOTE[1] line survey (Cernicharo et al. 2021a) and the Green Bank 100 m radio telescope with the GBT Observations of TMC-1: Hunting Aromatic Molecules (GOTHAM) survey (McGuire et al. 2018), demonstrates the great importance of this source for a complete understanding of the chemistry of the interstellar medium (ISM). Chemical models are not yet accurate enough to predict all the molecules that have been discovered, so we must continue to study the various chemical reactions in order to better constrain models of cold pre-stellar cores.

The TMC-1 cloud is remarkably rich in hydrocarbons, such as long carbon chains, propargyl (Agúndez et al. 2021), vinyl acetylene (Cernicharo et al. 2021b), and allenyl diacetylene (Fuentetaja et al. 2022). Furthermore, several cyclic molecules, such as indene, cyclopentadiene (Cernicharo et al. 2021c), ortho-benzyne (Cernicharo et al. 2021a), and fulvenallene (Cernicharo et al. 2022), have been discovered there.

The carbenes, a family of molecules discovered in the ISM, are characterized by having two non-bonded electrons located on a terminal carbon atom. The most relevant are the cumulene carbenes, whose formula is H_2C_n. They have a chain with double bonds between their carbon atoms. The simplest and the first to be discovered was l-H_2C_3, in 1991 (Cernicharo et al. 1991a). That same year, l-H_2C_4 was also discovered in TMC-1 (Kawaguchi et al. 1991) and IRC+10216 (Cernicharo et al. 1991b) . The longest species detected so far is l-H_2C_6, which has been found in several sources, including TMC-1 (Langer et al. 1997) and IRC+10216 (Guélin et al. 2000). Finally, Cabezas et al. (2021) detected l-H_2C_5 in TMC-1. For all of these molecules, the most stable isomer corresponds to the non-polar species with the formula HC_nH for an even n or a cyclic structure when n is odd. Several H_2C_n isomers have been detected in the ISM, such as c-C_3H_2 (Thaddeus et al. 1987) and c-C_3HCCH (Cernicharo et al. 2021c).

In the case of the C_6H_2 family, Sattelmeyer & Stanton (2000) performed the first theoretical study of the nine most stable isomers. They performed several types of ab initio calculations, the highest level being CCSD(T), using the cc-pVTZ basis set. The bent-chain isomer ethynylbutatrienyliden (HCCCHCCC) is 2.346 eV higher than the most stable isomer HC_6H, but only 0.1648 eV above the l-H_2C_6 species detected by Langer et al. (1997). Moreover, it should be noted that there are two isomers whose energy is lower than those of these two species. The formula is c-C_6H_2 for both of them, with the hydrogens in the ortho and meta positions (1.7085 eV and 2.0078 eV above the more stable isomer, respectively), making them possible candidates for future discovery.

On the other hand, if we consider sulphur-bearing species, we see that the number of molecules detected in TMC-1 is small compared with C- and O-rich species. However,

⋆ Based on observations carried out with the Yebes 40 m telescope (projects 19A003, 20A014, 20D023, 21A011, and 21D005). The 40 m radio telescope at Yebes Observatory is operated by the Spanish Geographic Institute (IGN, Ministerio de Transportes, Movilidad y Agenda Urbana).

[1] Q-band Ultrasensitive Inspection Journey to the Obscure TMC-1 Environment

Open Access article, published by EDP Sciences, under the terms of the Creative Commons Attribution License (https://creativecommons.org/licenses/by/4.0), which permits unrestricted use, distribution, and reproduction in any medium, provided the original work is properly cited.
This article is published in open access under the Subscribe-to-Open model. Subscribe to A&A to support open access publication.

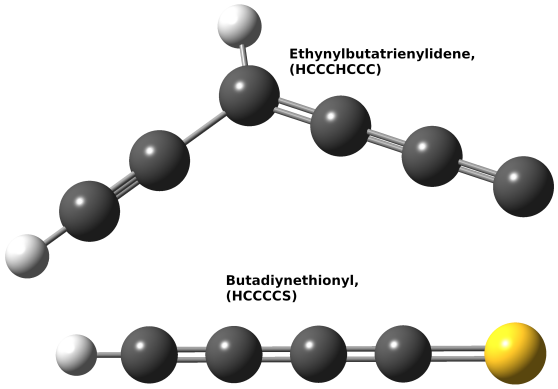

Fig. 1. Structure of the two molecules detected in this work.

some of them, such as CCS or CCCS, present a high abundance (Saito et al. 1987; Yamamoto et al. 1987). Among the last sulphur-bearing molecules discovered in TMC-1 we have HC_3S^+ (Cernicharo et al. 2021d), H_2CCS, H_2CCCS, NCS, HCCS, C_4S, and C_5S (Cernicharo et al. 2021e), the cation radical $HCCS^+$ (Cabezas et al. 2022), and the two derivatives of thioformaldehyde, HCSCN and HCSCCH (Cernicharo et al. 2021f).

In this Letter we report on the first identification of HCCCHCCC and HCCCCS towards TMC-1. We derive column densities and rotational temperatures for the two molecules and analyse them with our chemical models to explain which reactions can produce them.

2. Observations

The observational data used in this work are part of the ongoing QUIJOTE line survey, carried out with the Yebes 40 m telescope towards the cyanopolyyne peak of TMC-1 ($\alpha_{J2000} = 4^h41^m41.9^s$ and $\delta_{J2000} = +25°41'27.0''$). We used a new receiver built within the Nanocosmos project[2], which consists of two cold high electron mobility transistor amplifiers covering the 31.0–50.3 GHz band with horizontal and vertical polarizations. Receiver temperatures achieved in the 2019 and 2020 runs vary from 22 K at 32 GHz to 42 K at 50 GHz. Some power adaptation in the down-conversion chains effectively reduced the receiver temperatures in 2021 to 16 K at 32 GHz and 30 K at 50 GHz. The backends are $2 \times 8 \times 2.5$ GHz fast Fourier transform spectrometers with a spectral resolution of 38.15 kHz, providing full coverage of the Q band in both polarizations. A detailed description of the system is given by Tercero et al. (2021).

The data come from several observing runs carried out between December 2019 and May 2022, and correspond to 546 h of observing time on source, of which 293 and 253 h were acquired with a frequency-switching throw of 8 MHz and 10 MHz, respectively. A detailed description of the QUIJOTE line survey is provided in Cernicharo et al. (2021a). For each frequency throw, different local oscillator frequencies were used in order to remove possible side band effects in the down-conversion chain.

The telescope beam size is 56″ and 31″ at 31 and 50 GHz, respectively. The intensity scale used in this work, antenna temperature (T_A^*), was calibrated using two absorbers at different temperatures and the atmospheric transmission model ATM (Cernicharo 1985; Pardo et al. 2001). The adopted calibration uncertainties are at a level of 10%. The main beam efficiency varies from 0.6 at 32 GHz to 0.43 at 50 GHz (Tercero et al. 2021). All the data were analysed using the GILDAS package[3].

3. Results

For line identification, we used various catalogues, including CDMS (Müller et al. 2005), JPL (Pickett et al. 1998), and MADEX (Cernicharo 2012), which, as of September 2022, contained a total of 6434 spectral entries corresponding to the isotopologues and the ground and excited states of 1734 molecules.

3.1. Discovery of HCCCHCCC

Ethynylbutatrienyliden is a planar molecule with a nearly prolate top symmetry and whose electronic ground state corresponds to a singlet ^1A state (see Fig. 1). It was studied in the laboratory up to 40.3 GHz by McCarthy & Thaddeus (2002), who determined with high precision its rotational and centrifugal distortion constants (see Table B.1). The dipole moments, μ_a = 3.710D and μ_b = 1.320D, were obtained by Sattelmeyer & Stanton (2000). We fitted these lines and implemented the rotational constants and the dipole moment into MADEX (Cernicharo 2012). Twenty-nine lines of this species were found in our QUIJOTE data, with intensities between 0.5 and 1.2 mK. Derived line parameters are given in Table A.1 and the lines for $K_a \leq 1$ are shown in Fig. 2, while those corresponding to $K_a = 2$ are shown in Fig. 3. Some lines are blended, but the large number of them allows for a solid detection. From the observed frequencies in TMC-1, together with those measured by McCarthy & Thaddeus (2002), we obtained a new set of rotational constants (see Appendix B and Table B.1) with the FITWAT code, which uses a Watson asymmetric rotor Hamiltonian in I^r representation (Cernicharo et al. 2018). The merged fit provides very good frequency predictions below 50 GHz and realistic ones in the 50–100 GHz frequency range.

We used a model line fitting procedure (Cernicharo et al. 2018) to derive the column density and the rotational temperature assuming all rotational levels have the same T_{rot}. We adopted a source of uniform brightness with a diameter of 80″ from the C_6H maps presented in Fossé et al. (2001). We obtained $T_{rot} = 6 \pm 1$ K and $N(HCCCHCCC) = (1.3 \pm 0.2) \times 10^{11}$ cm^{-2}. To provide molecular abundances, we also assumed a H_2 column density for TMC-1 of 10^{22} cm^{-2} (Cernicharo & Guélin 1987), so the abundance of HCCCHCCC is $(1.3 \pm 0.2) \times 10^{-11}$. Figures 2 and 3 show the synthesized spectrum obtained with these values. The column density for the ortho species l-H_2C_6 is 6×10^{10} cm^{-2}, which, together with 2×10^{10} cm^{-2} for the para species, gives us a total column density $N(l\text{-}H_2C_6) = 8 \times 10^{10}$ cm^{-2} (Cabezas et al. 2021). Hence, the abundance ratio HCCCHCCC/l-H_2C_6 is 1.625. This species, with an angle between the carbon atoms of 123.63° (Sattelmeyer & Stanton 2000), could be a precursor of cyclic species.

3.2. Discovery of HCCCCS

Butadiynethionyl (HCCCCS) is a planar molecule with a $^2\Pi$ ground state. Line frequencies and the value of the dipole moment used are from the CDMS catalogue. The laboratory study of HCCCCS was carried out by Hirahara et al. (1994), who determined the value of B = 1434.298 MHz. The value of the dipole moment is $\mu = 1.45$D. We used these laboratory

[2] https://nanocosmos.iff.csic.es/

[3] http://www.iram.fr/IRAMFR/GILDAS

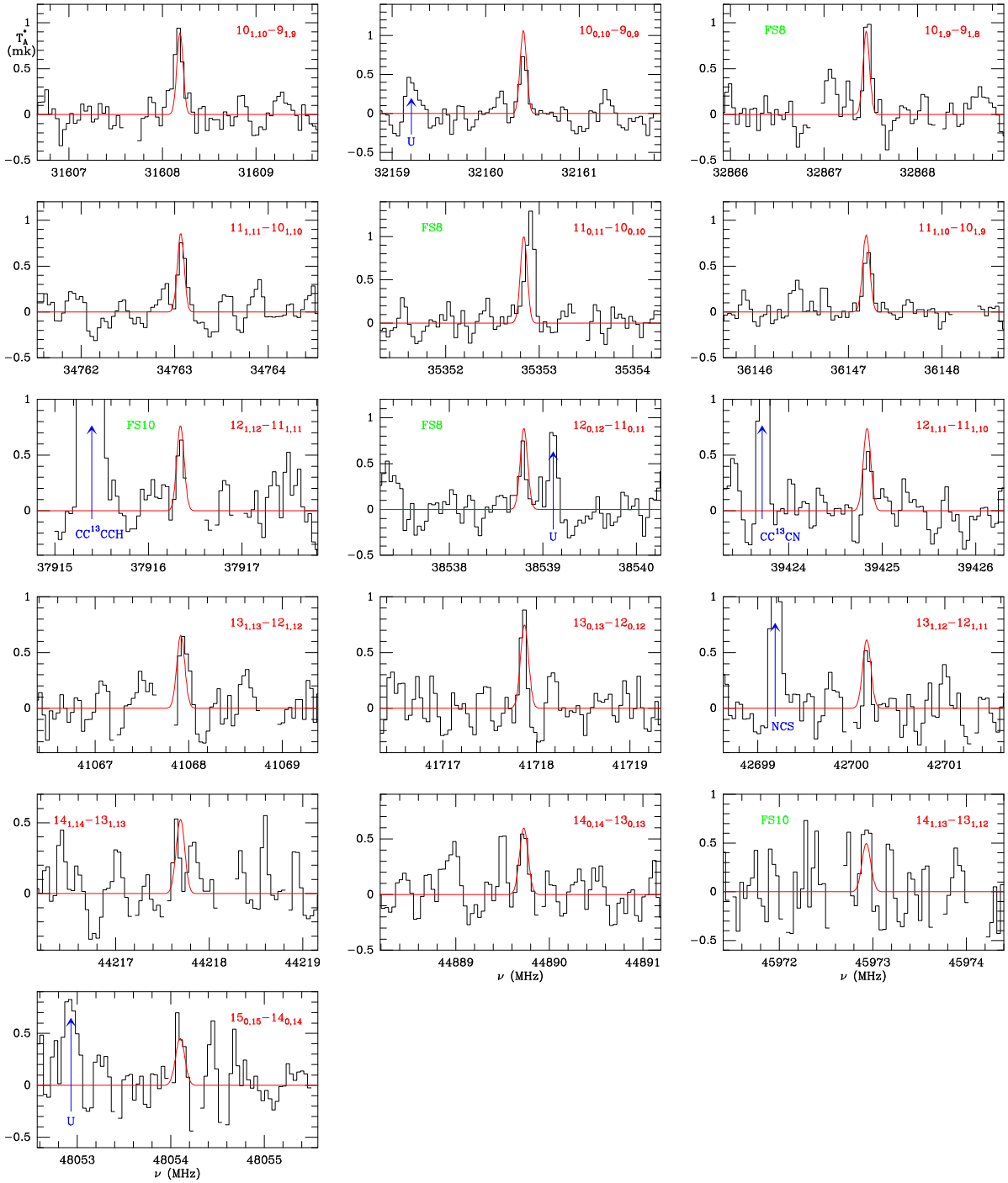

Fig. 2. Observed transitions $K_a = 0$ and 1 of HCCCHCCC in TMC-1. The abscissa corresponds to the rest frequency of the lines. Frequencies and intensities for the observed lines are given in Table A.1. The ordinate is the antenna temperature, corrected for atmospheric and telescope losses, in millikelvin. The quantum numbers of each transition are indicated in the corresponding panel. The red line shows the computed synthetic spectrum for this species for $T_{\rm rot} = 6\pm1$ K and a column density of $(1.3\pm0.2)\times10^{11}$ cm^{-2}. Blanked channels correspond to negative features produced when folding the frequency-switched data. Green labels indicate the transitions for which only one of the frequency-switching data have been used (FS10 and FS8 correspond to a throw of 10 and 8 MHz, respectively).

data to implement HCCCCS in the MADEX code and predict its rotational lines. We detected a total of six transitions, whose intensities ranged from 0.49 to 0.68 mK, as shown in Fig. 4. The derived line parameters are given in Appendix A. We obtained a rotational temperature of 10±1 K and a column density of $N = (9.5\pm0.8)\times10^{10}$ cm^{-2}. Smaller values of $T_{\rm rot}$ underestimate the intensity of the transitions at the highest frequencies. These derived parameters were used to obtain the synthetic spectrum shown in Fig. 4. Within the family HC_nS, the species HCS and HCCS have been detected with column densities of $5.5\pm0.5\times10^{12}$ cm^{-2} and $6.8\pm0.6\times10^{11}$ cm^{-2}, respectively (Cernicharo et al. 2021e). Therefore, the abundance ratios HCS/HCCCCS and HCCS/HCCCCS are 58 and 7.2, respectively. Propadienthionyl, HC_3S, has not been detected yet in the ISM. From the QUIJOTE line survey, we derived a 3σ upper limit to its column density of 5×10^{10} cm^{-2}.

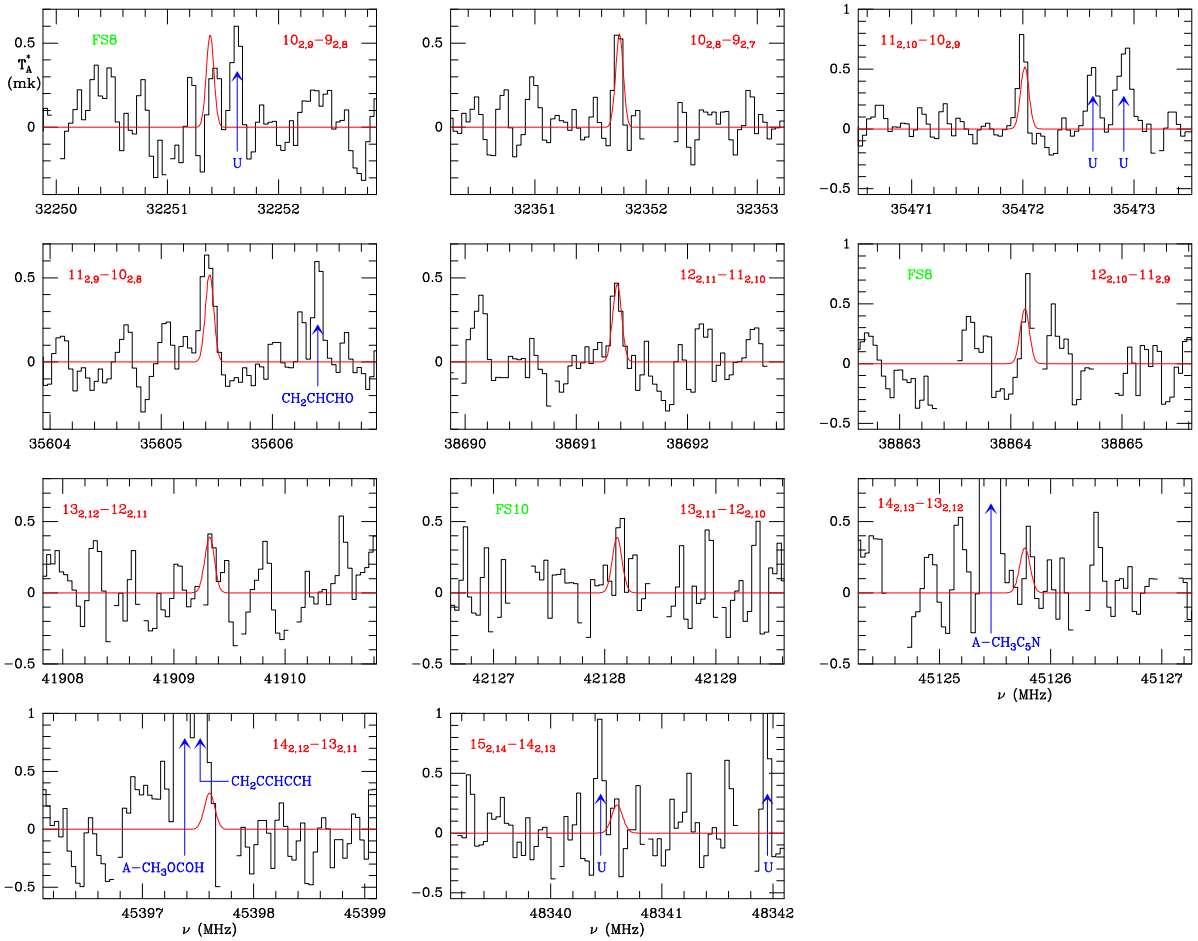

Fig. 3. Selected K_a = 2 transitions of HCCCHCCC in TMC-1. The abscissa corresponds to the rest frequency of the lines. Frequencies and intensities for all observed lines are given in Table A.1. The ordinate is the antenna temperature, corrected for atmospheric and telescope losses, in millikelvin. The quantum numbers of each transition are indicated in the corresponding panel. The red line shows the computed synthetic spectrum for this species for $T_{\rm rot} = 6\pm1$ K and a column density of $(1.3\pm0.2)\times10^{11}$ cm^{-2}. Blanked channels correspond to negative features produced when folding the frequency-switched data. Green labels indicate the transitions for which only one of the frequency-switching data have been used (FS10 and FS8 correspond to a throw of 10 and 8 MHz, respectively).

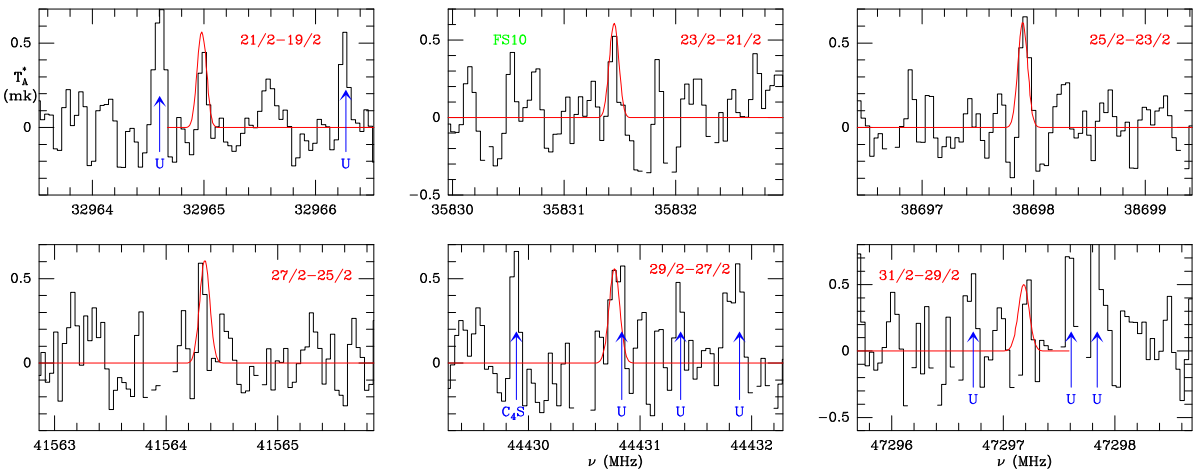

Fig. 4. Selected transitions of HCCCCS in TMC-1. The abscissa corresponds to the rest frequency of the lines. Frequencies and intensities for all observed lines are given in Table A.1. The ordinate is the antenna temperature, corrected for atmospheric and telescope losses, in millikelvin. The quantum numbers of each transition are indicated in the corresponding panel. The red line shows the computed synthetic spectra for this species for $T_{\rm rot} = 10$ K and a column density of $(9.5\pm0.8)\times10^{10}$ cm^{-2}. Blanked channels correspond to negative features produced when folding the frequency-switched data. Green labels indicate the transitions for which only one of the frequency-switching data have been used (FS10 corresponds to a throw of 10 MHz).

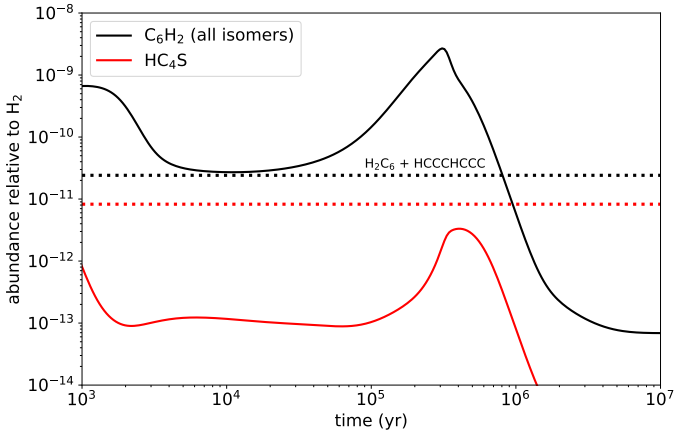

Fig. 5. Calculated fractional abundances of C_6H_2 (including all possible isomers) and HC_4S as a function of time. Horizontal dotted lines correspond to observed values in TMC-1; the dotted black lines account for the sum of the abundances of the two C_6H_2 isomers detected in TMC-1: H_2C_6 and HCCCHCCC. The most stable isomer, HC_6H, is probably the most abundant one, although it cannot be probed since it is non-polar.

4. Chemical model

We carried out chemical model calculations to shed light on the possible synthetic routes to HCCCHCCC and HC_4S. The model parameters and chemical network used are similar to those employed by Cernicharo et al. (2021e) to model the chemistry of sulphur-bearing molecules. Modifications to the chemical network are described below.

We first focused on the hydrocarbon HCCCHCCC. This species is an isomer of the C_6H_2 family. The most stable isomer, HC_6H, is probably the most abundant one, although it cannot be detected because it is non-polar, while the cumulene isomer H_2C_6 is detected in TMC-1 with an abundance somewhat lower than that of HCCCHCCC. Due to the lack of information on the chemical kinetics of the different C_6H_2 isomers, the chemical networks do not differentiate between them. In the chemical model, the most important reactions of C_6H_2 formation are: $C_6H^- + H$, the dissociative recombination of $C_6H_3^+$, and the neutral-neutral reaction $C_4H + C_2H_2$. The first and last reactions have been measured and determined to be rapid (Eichelberger et al. 2007; Berteloite et al. 2010), although information on the branching ratios of the different C_6H_2 isomers is not available. The dissociative reaction has not been measured, so the kinetic coefficient and the fragmentation channels used are an estimation determined by Herbst & Leung (1989). Given that the calculated abundance of all isomers of C_6H_2 is well above the sum of the observed abundances of H_2C_6 and HCCCHCCC (see Fig. 5) and that the undetected isomer HC_6H is probably the most abundant one, it is likely that H_2C_6 and HCCCHCCC are formed by any of the aforementioned reactions, with branching ratios lower than the one that forms HC_6H. Information on the product distribution for these reactions would allow light to be shed on the chemistry of C_6H_2 isomers.

The sulphur-bearing species HC_4S is not included in chemical networks (e.g., Vidal et al. 2017). We thus included it assuming standard destruction routes (through reactions with neutral atoms and cations) and formation through $C + H_2C_3S$ (in analogy to the reaction $C + H_2CS$, which is the main route to HCCS; Cernicharo et al. 2021e) and by the dissociative recombination of $H_2C_4S^+$, where this cation is in turn assumed to form through the reactions $S + C_4H_3^+$ and $S^+ + C_4H_3$. The calculated peak abundance of HC_4S is in reasonable agreement with the value observed in TMC-1 (see Fig. 5), which supports the idea that this species is formed through neutral and ionic routes similar to those that form other S-bearing carbon chains (Vidal et al. 2017; Cernicharo et al. 2021e).

5. Conclusions

We report on the detection of HCCCHCCC and HCCCCS towards the cold dark cloud TMC-1. For the former, we derived a column density of $(1.3\pm0.2)\times10^{11}$ cm^{-2} with $T_{\rm rot} = 6\pm1$ K. HCCCHCCC is thus more abundant than its cumulene isomer, which allows the chemistry of the C_6H_2 family to be constrained. For the sulphur-bearing molecule, we obtained a column density of $(9.5\pm0.8)\times10^{10}$ cm^{-2} with $T_{\rm rot} = 10$ K. According to our chemical model, this abundance can be correctly approximated with the standard destruction and formation routes.

Acknowledgements. We thank Ministerio de Ciencia e Innovación of Spain (MICIU) for funding support through projects PID2019-106110GB-I00, PID2019-107115GB-C21/AEI/10.13039/501100011033, and PID2019-106235GB-I00. We also thank ERC for funding through grant ERC-2013-Syg-610256-NANOCOSMOS. M.A. thanks MICIU for grant RyC-2014-16277.

References

Agúndez, M., Cabezas, C., Tercero, B., et al. 2021, A&A, 647, L10
Berteloite, C., Le Picard, S., Balucani, N., et al. 2010, PCCP, 12, 3677
Cabezas, C., Tercero, B., Agúndez, M., et al. 2021, A&A, 650, L9
Cabezas, C., Agúndez, M., Marcelino, N., et al. 2022, A&A, 657, L4
Cernicharo, J. 2012, in ECLA 2011: Proc. of the European Conference on Laboratory Astrophysics, eds. C. Stehl, C. Joblin, & L. d'Hendecourt (Cambridge: Cambridge Univ. Press), EAS Pub. Ser., 251
Cernicharo, J. 1985, Internal IRAM report (Granada: IRAM)
Cernicharo, J., & Guélin, M. 1987, A&A, 176, 299
Cernicharo, J., Gottlieb, C. A., Guélin, M., et al. 1991a, ApJ, 368, L39
Cernicharo, J., Gottlieb, C. A., Guélin, M., et al. 1991b, ApJ, 368, L43
Cernicharo, J., Guélin, M., Agúndez, M., et al. 2018, A&A, 618, A4
Cernicharo, J., Agúndez, M., Kaiser, R., et al. 2021a, A&A, 652, L9
Cernicharo, J., Agúndez, M., Cabezas, C., et al. 2021b, A&A, 647, L2
Cernicharo, J., Agúndez, M., Cabezas, C., et al. 2021c, A&A, 649, L15
Cernicharo, J., Cabezas, C., Endo, Y., et al. 2021d, A&A, 646, L3
Cernicharo, J., Cabezas, C., Agúndez, M., et al. 2021e, A&A, 648, L3
Cernicharo, J., Cabezas, C., Endo, Y., et al. 2021f, A&A, 650, L1
Cernicharo, J., Fuentetaja, R., Agúndez, M., et al. 2022, A&A, 663, L9
Eichelberger, B., Snow, T. P., Barckholtz, C., & Bierbaum, V. M. 2007, ApJ, 667, 1283
Fossé, D., Cernicharo, J., Gerin, M., & Cox, P. 2001, ApJ, 552, 168
Fuentetaja, R., Cabezas, C., Agúndez, M., et al. 2022, A&A, 663, L3
Guélin, M., Müller, S., & Cernicharo, J. 2000, A&A, 363, L9
Herbst, E., & Leung, C. M. 1989, ApJ, 69, 271
Hirahara, Y., Ohshima, Y., & Endo, Y. 1994, J. Chem. Phys., 101, 7342
Kawaguchi, K., Kaifu, N., Ohishi, M., et al. 1991, PASJ, 43, 607
Langer, W. D., Velusamy, T., Kuiper, T. B. H., et al. 1997, ApJ, 480, L63
McCarthy, M. C., & Thaddeus, P. 2002, ApJ, 569, L55
McGuire, B. A., Burkhardt, A. M., Kalenskii, S., et al. 2018, Science, 359, 202
Müller, H. S. P., Schlöder, F., Stutzki, J., & Winnewisser, G. 2005, J. Mol. Struct., 742, 215
Pardo, J. R., Cernicharo, J., & Serabyn, E. 2001, IEEE Trans. Anten. Propag., 49, 12
Pickett, H. M., Poynter, R. L., Cohen, E. A., et al. 1998, J. Quant. Spectrosc. Radiat. Transf., 60, 883
Saito, S., Kawaguchi, K., Yamamoto, S., et al. 1987, ApJ, 317, L1156
Sattelmeyer, K. W., & Stanton, J. F. 2000, J. Am. Chem. Soc., 122, 8220
Tercero, F., López-Pérez, J. A., Gallego, J. D., et al. 2021, A&A, 645, A37
Thaddeus, P., Vrtilek, J. M., & Güttlieb, C. A. 1987, ApJ, 299, L63
Vidal, T. H. G., Loison, J.-C., Jaziri, A. Y., et al. 2017, MNRAS, 469, 435
Yamamoto, S., Saito, S., Kawaguchi, K., et al. 1987, ApJ, 317, L119

Appendix A: Observed line parameters

We obtained the observed line parameters for the two molecules detected in this work by fitting a Gaussian line profile to the observed data, using CLASS (GILDAS package). For this purpose, we considered a window of ±15 km s^{-1} around the V_{LSR} (5.83 km s^{-1}) of the source for each transition. The results are shown in Table A.1. Observed lines of HCCCHCCC are shown in Figs. 2 and 3, and lines of HCCCCS in Fig. 4. Some of these parameters correspond to lines with only frequency-switching data with a throw of 8 or 10 MHz. In other cases, the lines are partially blended, but we can derive good parameters. For lines that are marginally detected, an upper limit of 3σ is given (see Notes).

Table A.1. Observed line parameters for the species studied in this work.

Transition	ν_{rest} [a] (MHz)	$\int T_A^* dv$ [b] (mK km s^{-1})	Δv [c] (km s^{-1})	T_A^* [d] (mK)	Notes
		HCCCHCCC[1]			
$10_{1,10}$-$9_{1,9}$	31608.167±0.010	1.08±0.17	1.20± 0.26	0.85±0.13	
$10_{0,10}$-$9_{0,9}$	32160.402±0.010	0.81±0.11	1.00± 0.16	0.76±0.11	
$10_{2,9}$-$9_{2,8}$	32251.428±0.020	0.25±0.11	0.74± 0.27	0.31±0.13	B
$10_{2,8}$-$9_{2,7}$	32351.748±0.010	0.44±0.08	0.64± 0.13	0.64±0.11	
$10_{1,9}$-$9_{1,8}$	32867.458±0.010	0.92±0.11	0.77± 0.11	1.12±0.15	B
$11_{1,11}$-$10_{1,10}$	34763.081±0.010	0.70±0.14	0.87± 0.20	0.75±0.15	
$11_{0,11}$-$10_{0,10}$	35352.883±0.010	0.95±0.14	1.13± 0.18	0.79±0.12	B
$11_{2,10}$-$10_{2,9}$	35471.993±0.010	0.57±0.09	0.64± 0.10	0.83±0.11	
$11_{2,9}$-$10_{2,8}$	35605.414±0.010	0.76±0.10	1.07± 0.16	0.67±0.13	
$11_{1,10}$-$10_{1,9}$	36147.207±0.010	0.22±0.07	0.53± 0.15	0.38±0.12	
$12_{1,12}$-$11_{1,11}$	37916.331±0.010	0.42±0.11	0.63± 0.18	0.63±0.20	C
$12_{0,12}$-$11_{0,11}$	38538.774±0.015	0.60±0.14	1.15± 0.36	0.49±0.13	B
$12_{2,11}$-$11_{2,10}$	38691.356±0.010	0.41±0.09	0.79± 0.19	0.49±0.13	
$12_{2,10}$-$11_{2,9}$	38864.149±0.010	0.41±0.13	0.49± 0.13	0.78±0.20	B
$12_{1,11}$-$11_{1,10}$	39424.853±0.015	0.40±0.08	0.67± 0.14	0.56±0.14	
$13_{1,13}$-$12_{1,12}$	41067.952±0.010	0.54±0.11	0.75± 0.16	0.67±0.17	
$13_{0,13}$-$12_{0,12}$	41717.861±0.010	0.49±0.10	0.47± 0.12	0.98±0.14	
$13_{2,12}$-$12_{2,11}$	41909.344±0.015	0.29±0.10	0.49± 0.25	0.56±0.15	
$13_{2,11}$-$12_{2,10}$	42128.143±0.010	0.26±0.06	0.34± 0.15	0.70±0.21	C
$13_{1,12}$-$12_{1,11}$	42700.173±0.010	0.26±0.08	0.36± 0.27	0.69±0.17	
$14_{1,14}$-$13_{1,13}$	44217.650±0.010	0.26±0.09	0.46± 0.16	0.53±0.17	
$14_{0,14}$-$13_{0,13}$	44889.725±0.015	0.28±0.11	0.51± 0.21	0.51±0.17	
$14_{2,13}$-$13_{2,12}$	45125.808±0.020	0.21±0.10	0.39± 0.21	0.50±0.20	
$14_{2,12}$-$13_{2,11}$	45397.603±0.080				A
$14_{1,13}$-$13_{1,12}$	45972.928±0.015	0.57±0.18	0.64± 0.19	0.83±0.33	C
$15_{1,15}$-$14_{1,14}$	47365.640±0.020	0.15±0.10	0.37± 0.19	0.38±0.24	
$15_{0,15}$-$14_{0,14}$	48054.091±0.020	0.39±0.15	0.57± 0.23	0.64±0.24	
$15_{2,14}$-$14_{2,13}$	48340.579±0.010	0.12±0.06	0.26± 0.09	0.45±0.23	
$15_{1,14}$-$14_{1,13}$	49242.813±0.010			≤0.57	D
		HCCCCS[2]			
21/2-19/2	32964.992± 0.010	0.32±0.11	0.61± 0.17	0.49±0.14	
23/2-21/2	35831.439± 0.010	0.27±0.08	0.44± 0.20	0.57±0.16	C
25/2-23/2	38697.923± 0.010	0.48±0.10	0.64± 0.12	0.70±0.15	
27/2-25/2	41564.324± 0.010	0.27±0.05	0.30± 0.12	0.83±0.16	
29/2-27/2	44430.777± 0.010	0.44±0.09	0.68± 0.16	0.61±0.16	
31/2-29/2	47297.214± 0.010	0.21±0.05	0.25± 0.42	0.78±0.22	

Notes. [(1)]Quantum numbers are $J'_{K'_a,K'_c}$ - J_{K_a,K_c}. [(2)]Quantum numbers are J'-J. [(a)]Observed frequency of the transition assuming a local standard of rest velocity of 5.83 km s^{-1}. [(b)]Integrated line intensity in mK km s^{-1}. [(c)]Linewidth at half intensity derived by fitting a Gaussian function to the observed line profile (in km s^{-1}). [(d)]Antenna temperature in millikelvin. [(A)]This line is fully blended with a transition of $CH_2CCHCCH$. The frequency corresponds to that calculated with the laboratory constants of Table B.1. [(B)]Frequency-switching data with a throw of 8 MHz only. Negative feature present in the data with a 10 MHz throw. [(C)]Frequency-switching data with a throw of 10 MHz only. Negative feature present in the data with a 8 MHz throw. [(D)]Upper limit corresponds to 3σ.

Appendix B: Improved rotational constants for HCCCHCCC

We merged the laboratory lines of HCCCHCCC obtained by McCarthy & Thaddeus (2002) with those observed in TMC-1. This improves the values of the rotational and distortion constants. The results are given in Table B.1. The values obtained from the merged fit are very similar to those obtained from the laboratory fit, with the greatest difference being less than 1 kHz.

Table B.1. Improved rotational and distortion constants for HCCCHCCC.

Constant (MHz)	Theoretical[1]	Laboratory[2]	Lab + TMC-1[3]
A	21399.8	21094.10161(25)	21094.10153(52)
B	1664.0	1676.268423(70)	1676.26835(81)
C	1543.9	1550.066623(42)	1550.066695(60)
$\Delta_J \times 10^3$	0.579	0.6414(77)	0.64165(44)
Δ_{JK}	-0.0662	-0.075808(14)	-0.075820(25)
$\delta_J \times 10^3$	0.144	0.16067(50)	0.15976(52)
J_{max}		7	15
$K_{a,max}$		1	2
N_{lines}		24	49
σ (kHz)		0.5	1.5
ν_{max} (MHz)		40330	48340

Notes. [(1)]Ab initio calculation from Sattelmeyer & Stanton (2000). [(2)]Rotational and distortion constants derived from a fit to the laboratory data of McCarthy & Thaddeus (2002). [(3)]Rotational and distortion constants derived from a merged fit to the laboratory and TMC-1 frequencies.